Design and Analysis of A New GaN-Based AC/DC Topology for Battery Charging Application

Akrem M. Elrajoubi, Kenny George, Simon S. Ang
Dept. of Electrical Engineering, University of Arkansas, Fayetteville, AR 72701
amelrajo@uark.edu, jkg001@uark.edu, siang@uark.edu

***Abstract*— Gallium nitride (GaN) technology reduces switching losses and allows faster device switching speeds. Meanwhile, high frequency (HF) transformers feature reduced weight and size for many applications. In this paper a new GaN-based power supply topology for battery charging applications is designed, simulated, analyzed, and constructed. The proposed topology is designed for 120Vac to 48Vdc/60Vdc conversion, operating at 100 KHz in the 1.3–1.5 kW range. A totem-pole power-factor-correction (TP-PFC) active front-end is utilized to yield close-to-unity power factor (~0.98) and higher efficiency with reduced harmonic content. This work designs and analyzes a new topology to combine the advantages of GaN TP-PFC and a high-frequency series resonant converter (SRC) with current doubler rectifier (CDR) utilizing the superior switching characteristics of GaN devices and the reduced size and cost of HF transformer. A loss-free resistor model is used to determine keys steady state and the main characteristics of the proposed topology.**

Keywords— Gallium nitride topology analysis and simulation; totem-pole power-factor corrector; series resonant converter; current doubler rectifier.

I. INTRODUCTION

With the current advancement in wide bandgap power semiconductors, power conversion with HF-link has been found very convenient for many applications, and it gives an opportunity to improve the power density and efficiency as well as reducing the weight, volume, and cost. GaN technology is significant as GaN HEMT devices have smaller ON resistances, and thus, smaller conduction losses. Also, near-zero reverse recovery charge losses in hard-switched converters makes totem-pole PFCs feasible [1], [2]. A 1 MHz totem-pole bridgeless PFC rectifier has been designed in [1] using the low-loss 600V GaN device, which provides a great front-end converter for low power applications. On the other hand, the CDR reduces RMS current on the transformer secondary (half of the load current, so less copper losses) and, hence, the output voltage ripple is reduced. Therefore, it is widely used for high current, low voltage applications. Also, CDR yields smaller leakage inductance to achieve zero-voltage-switching (ZVS) condition [3], [4], it has bi-directional energy control capability, and offers a better thermal performance (good heat dissipation). CDR also has an improved transient response [5]. Reference [6] designed an optimized telecom phase shift full-bridge DC–DC converter with CDR for 400Vdc input voltage, while the proposed topology in this paper utilizes the 120 Vac line input and SRC, which is easier to control and yields half of the voltage to the transformer primary side. Most importantly, converter losses in series resonant converters are drastically reduced due to zero-voltage- and zero-current-switching operations of all switching devices compared to hard-switching full-bridge and half-bridge topologies, which increases the overall efficiency of this proposed topology. The combination of the reduced SRC losses with the alleviation of losses in the transformer secondary winding, due to the CDR, makes the proposed topology a very attractive high-efficiency battery charging solution.

II. DESIGNED GAN AC/DC TOPOLOGY

Fig. 1 shows the proposed GaN based AC/DC converter topology to provide 48Vdc to 60Vdc output employing a totem-pole bridgeless PFC front-end, series-resonant converter, and current-doubler rectifier output. This topology lends itself to high-frequency operation with reduced losses in the PFC stage due to the lack of a full-bridge rectifier and through the use of GaN MOSFET devices. In addition, by using a current-doubler rectifier, conduction losses in the transformer secondary winding are reduced. Simulation of the proposed power supply topology was performed using MATLAB/Simulink after the design of the main components (shown in Table 1). Fig. 2 demonstrates the key simulation waveforms and the output voltage of the proposed topology. Then the controllers are designed as shown in Fig. 3 to maintain a close-to-unity power factor, low harmonic contents, and high efficiency converter. In reference [7], Transphorm Inc. demonstrates a GaN-based PFC using average current mode (ACM) control, combined with outer voltage loop control and input voltage feed forward to achieve 99% efficiency and >0.98 power factor. This controller architecture increases converter robustness, while also minimizing THD (<5% based on simulation) on the AC-link. The SRC and CDR must operate as deemed necessary by the connected battery; a combination of output current regulation and voltage measurement is employed to safely and quickly charge a battery tank. A loss-free resistor (LFR) model for the PFC, and a First Harmonic Approximation (FHA) model for the SRC of the proposed topology are first derived to expedite the design and analysis of the output voltage and current compensators for battery charging applications. Texas Instruments™ TMS320F28335 DSP controller is used in the experimental prototype as code generation, debugging and running can be accomplished for the topology control algorithm.

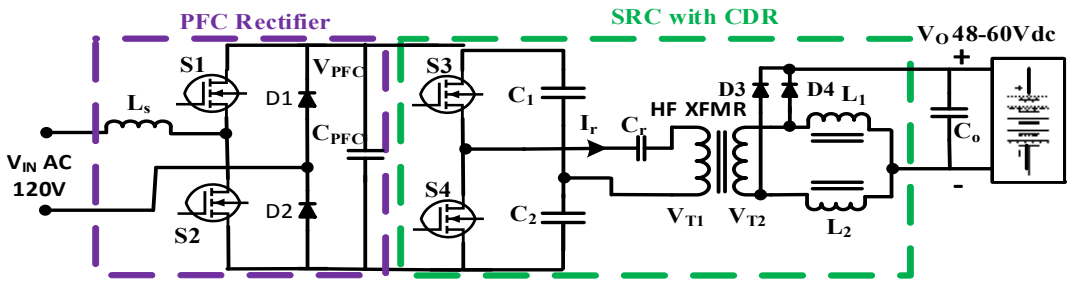

Fig. 1. The proposed GaN-based AC/DC Converter Topology.

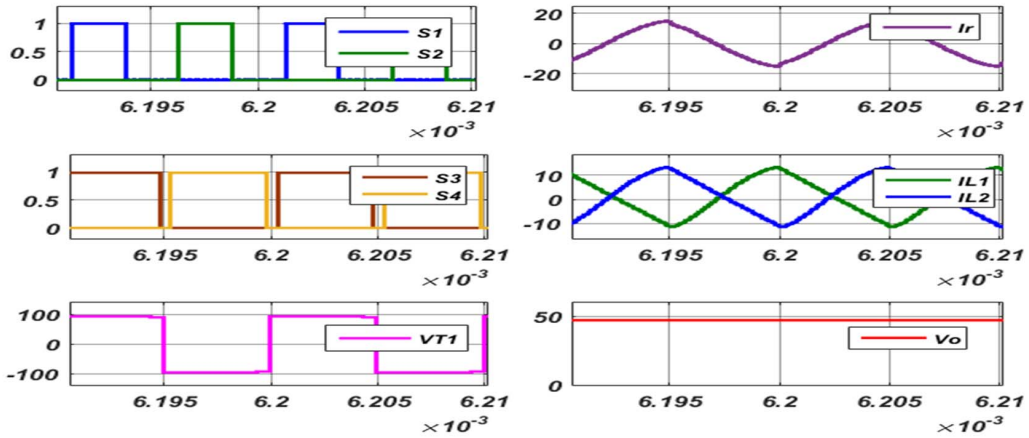

Fig. 2. Key Simulation Waveforms of the Proposed Topology.

TABLE I. TOPOLOGY DESIGN EQUATIONS AND COMPONENT VALUES.

DESIGN EQUATIONS	COMPONENT	VALUE	COMPONENT	VALUE
$M = 1 - D = \frac{\sqrt{2}\, V_{in-rms}}{V_{o_{pfc}}}$	C_{PFC}	47 µF	HF-XFMR Turns Ratio	10:9
$L_s = \frac{\sqrt{2}\, V_{in-rms}\, D}{f_{sw}\, i_{ripple}}$, $L_1 = L_2 = \frac{(V_s - V_{out})D}{f_{sw}\, \Delta i_L}$ [8]	C_1, C_2	6.8 µF	L_s, L_1, L_2	270µH, 10µH, 10µH
$C_r = \frac{1}{L_r(2\pi f_{sw})^2}$, $C_o = \frac{i_L}{2\pi f_{sw} V_{out}}$	C_r	0.22 µF	C_o	6600 µF

Fig. 3 shows the control of the proposed topology for battery charging applications requires the PFC to rectify the AC input at near-unity power factor to feed the DC-DC converter stage – this is one set of controls for the converter that will be described. The SRC operates as a voltage/current regulator for charging the battery using variable-frequency control. The PFC is controlled using average current mode control with an input voltage feed forward path that provides a waveform shape for the inductor current to track. Combined with sensing of the current waveform, this will be referred to as the current loop control. The current is sensed using a low-valued resistor and is filtered using an op-amp based low-pass filter (G_{sense}). This measured current is compared to a reference and fed into a controller (G_{ci}) which drives the PWM output of the loop. Equations used to describe this loop are given below along with the duty cycle to inductor current transfer function (G_{id}) and the total loop gain (G_i).

$$G_{sense} = \frac{R_S}{1+\frac{s}{\omega_{si}}} \quad (1)$$

$$G_{id} = \frac{V}{sL_s} \quad (2)$$

$$G_i = G_{sense} G_{ci} G_{id} \quad (3)$$

where V is the nominal output voltage of the PFC, L_s is the input inductor, R_s is the sensing resistor, and ω_{si} is the

cutoff frequency of the sensing filter. Output voltage of the PFC is regulated using a low-bandwidth outer voltage loop. The outer voltage loop is described as a function of the energy stored in the capacitor. As described in [9], under constant power load, which is assumed here given the constant current and constant voltage charging modes of the battery, the voltage loop gain is given as:

$$G_v = \frac{P_{load} V_{fb}}{sC_o V V_{control}} \tag{4}$$

where V_{fb} is the feedback attenuation, P_{load} is the rated power of the load, and $V_{control}$ is the reference voltage at the output given as:

$$V_{control} = \frac{2R_s P_{load} V_{fb}}{k_v} \tag{5}$$

where k_v is a constant of proportionality term in the current loop tracking reference. This term is often large when using high feedback voltage attenuation.

The SRC with CDR has been studied in [10]. Using the model derived in [10], the converter can be modeled quite simply. The input to output transfer function of the SRC with CDR is given as:

$$\frac{v_o}{v_i} = \left| \frac{s^2 2nC_b R_e}{s^3 C_b L_{lk} + s^2 C_b R_e c + s + \frac{R_e}{L_1}} \right| \tag{6}$$

with R_e being the equivalent load, n being the transformer turns ratio, L_{lk} is transformer leakage inductance functioning as the resonant inductance, and L_1 being the coupled inductor inductance. The term c is described as a relationship between the mutual inductance of the coupled inductor, its intrinsic inductance, and resonant inductance:

$$c = 4 + \frac{L_{lk}}{L_1} \tag{7}$$

Note that the magnetizing inductance is assumed to be large and does not affect the model in any way, though it was included in [10] in their use of the LLC resonant converter. The bode plot of this transfer function shows that it follows closely the voltage conversion plot associated with the SRC using the fundamental harmonic analysis. Regulation of the output is attained through the use of a PI controller which is able to regulate current to match the charging current of a given battery charging profile. Fig. 4 shows the PFC current loop gains for the controller's design and SRC with CDR Bode plots.

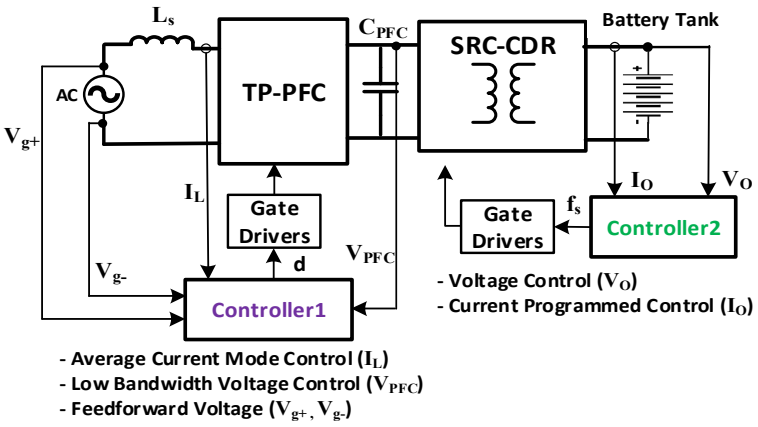

Fig. 3. The Controller Diagram for the proposed Topology.

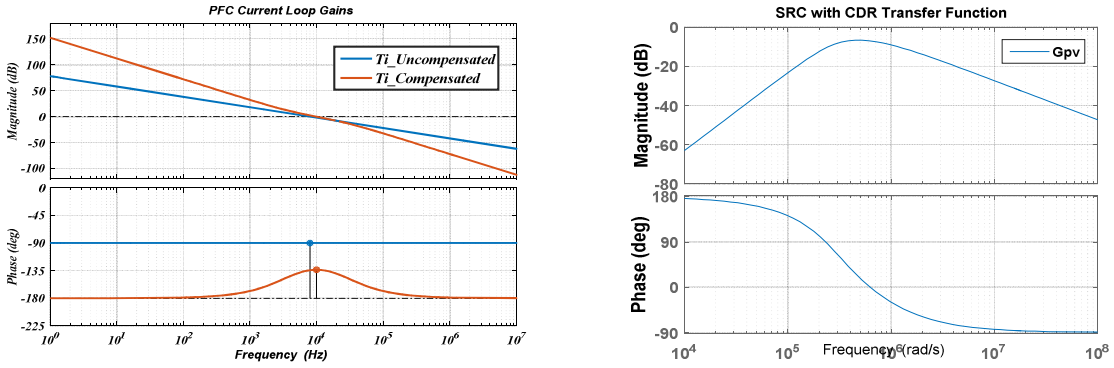

Fig. 4. PFC Current Controller and SRC with CDR Bode Plots.

It is desired to have very good dynamic performance to avoid stability issues for this nonlinear system. An averaged model and state space model for the converter under consideration are used to obtain stable steady state performance and transient responses.

III. TOPOLOGY SIMULATION AND MODELING

Examination of the equivalent circuit model for each PFC half-cycle of operation shows that it exhibits identical operation as that of a bridge-rectifier based boost PFC. Thus, an equivalent model of the totem-pole PFC is used that is the same as the traditional bridge-rectified boost PFC to design average current mode control to maintain a close-to- unity power factor, and low harmonic components as shown in the simulation waveforms of Fig. 5. The simulation results show that the PFC attains near unity power factor and stable operation with a 200V dc-link sustained for conversion by the SRC. Similarly, the SRC with CDR is able to regulate the charging current and voltage of the battery. Both the switching model and the averaged model yield an average PFC voltage of 200V, the input current is in phase with the ac input voltage.

Fig. 6 shows the output voltage for a battery model while the battery charging current is controlled with an average current mode control. Fig. 7 demonstrates the SRC gate pluses and discontinuous conduction mode (DCM) current for the resonant tank. DCM for the SRC is more convenient to regulate the output charging current. However, for soft switching operation the SRC is subjected to switching frequency modulating. Also, applying fixed frequency PWM control schemes to switches S_3, S_4 enables adjusting the CDR current and output voltage. Fig. 8 depicts the equivalent averaged model for the entire proposed topology. As shown, M is the HF transformer primary and secondary mutual inductance. The PFC is presented as a two port model for the ideal rectifier called loss-free resistor (LFR) model, while the SRC is modeled by the equivalent First Harmonic Approximation (FHA) method as documented in [9]. Then the CDR is modeled for positive coupling configuration as explained in [10] for the coupled inductor. The averaged state space model for the equivalent simplified steady state operating modes of the proposed topology and its transfer function are shown in Fig. 9. This state space model is a mathematical model derived to obtain an average description of the topology for one switching cycle to present the main modes of operation. The state variables are PFC inductor (L_s) current, C_1, and C_2 voltages, resonant (transformer primary side) current, and resonant capacitor voltage. The main modes of operation are analyzed for the topology by considering the switches pulses of the key waveforms presented in Fig. 2.

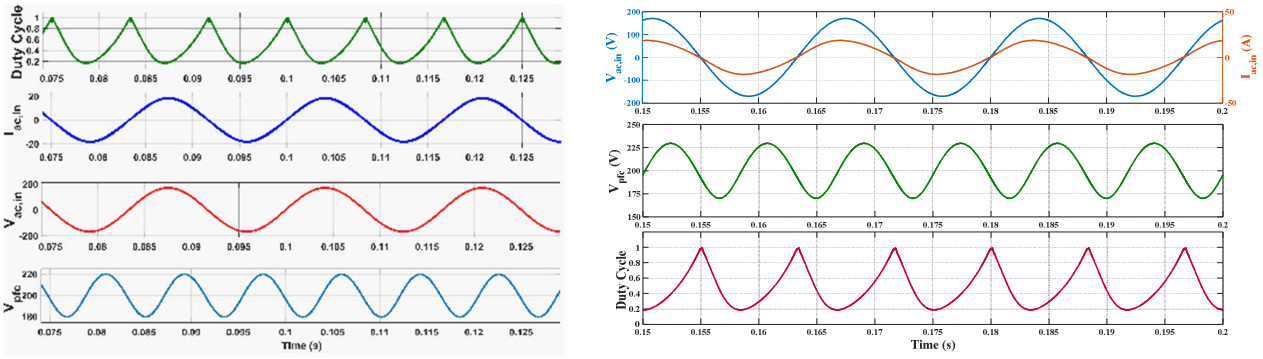

a. The switching model

b. The averaged model

Fig. 5. PFC Average Current Mode Control Simulation Waveforms.

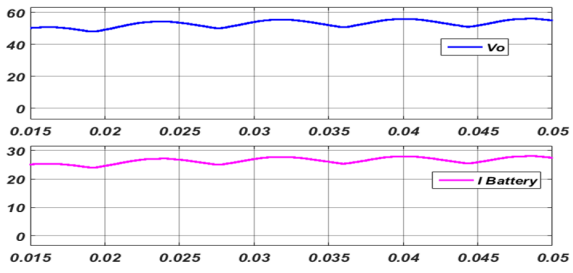

Fig. 6. Battery Voltage and Average Charging Current.

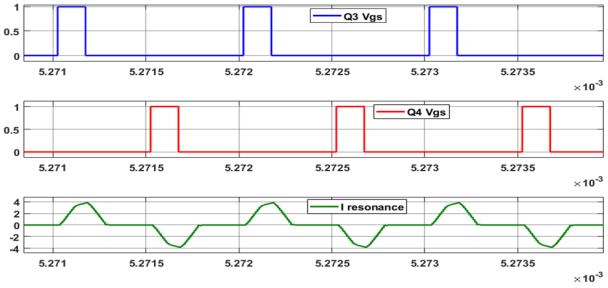

Fig. 7. SRC Gate Pulses and DCM Resonant Tank Current.

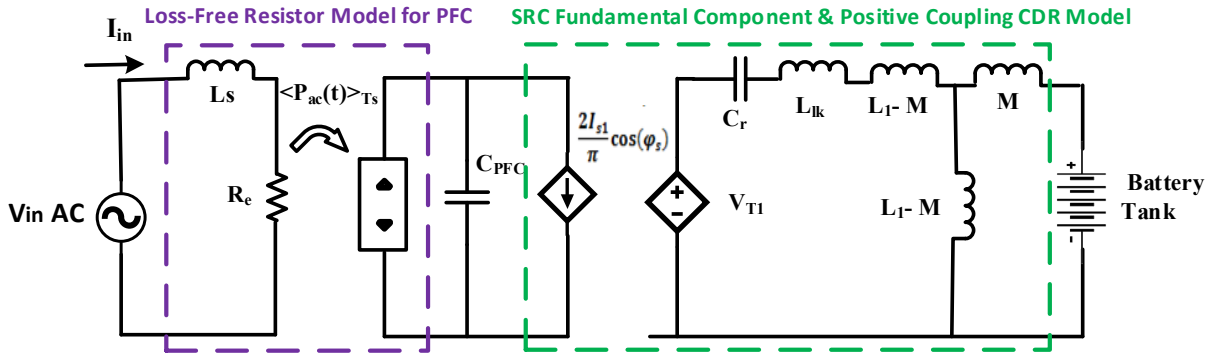

Fig. 8. The Equivalent Model for the proposed Converter.

$$\dot{X} = \begin{bmatrix} 0 & \frac{-1}{L_s} & \frac{-1}{L_s} & 0 & 0 \\ \frac{1}{C_1} & 0 & 0 & 0 & 0 \\ \frac{1}{C_2} & 0 & 0 & \frac{-n}{C_2} & 0 \\ 0 & 0 & \frac{1}{nL_{lk}+2L/n} & 0 & \frac{-1}{nL_{lk}+2L/n} \\ 0 & 0 & 0 & \frac{n}{C_r} & 0 \end{bmatrix} \begin{bmatrix} i_s \\ V_{c1} \\ V_{c2} \\ i_r \\ V_{cr} \end{bmatrix} + \begin{bmatrix} \frac{1}{L_s} \\ 0 \\ 0 \\ 0 \\ 0 \end{bmatrix} U$$

$$Y = V_{out} = \begin{bmatrix} 0 & 0 & \frac{L}{n^3 L_{lk}+2Ln} & 0 & \frac{-L}{n^3 L_{lk}+2Ln} \end{bmatrix} X$$

$$T(s) = \frac{L\,S^2}{\Delta C L_s\,(n^3\,L_{lk} + 2nL)}$$

Where Δ is the determint of (SI − A):

$$\Delta = S^4 + \frac{2\,S^2}{CL_s} + \frac{n}{(nL_{lk}+{}^{2L}/_{n})}\left[\frac{S^2}{C_r} + \frac{S^2}{C} + \frac{2}{CC_rL_s} + \frac{1}{C^2L_s}\right].$$

Where: $C_1 = C_2 = C$, $L_1 = L_2 = L$, L_{lk} is transformer leakage inductance, and n is its turn ratio.

Fig. 9. The Averaged State Space Model for the proposed Converter and its Transfer Function.

IV. TOPOLOGY DESCRIPTION AND OPERATION

Both zero-voltage switching and zero-current switching are implemented in the series resonant converter to minimize switching stresses as well as switching power loss. The resonance frequency and the characteristic impedance depend on the values of the resonant capacitor and the transformer leakage inductance. The quality factor Q of the proposed topology is given by:

$$Q = \sqrt{L_r / C_r} / R_{Load} \quad (8)$$

For the proposed topology, a 100 KHz transformer is designed with optimum specifications as shown in Table 2. The GaN transistors S_1 to S_4 in this design prototype are GS66504B 15 A 650 V E-mode GaN transistors, while half bridge gate driver for E mode GaN FETs (LM5113 100 V 1.2-A / 5-A) is used to drive both the high and bottom switching positions. A low profile, high current coupled 10µH inductor is used for the CDR as the coupled inductor will not influence the overall resonant converter behavior as the gain characteristics of the resonant converter are relatively unaffected [10]. The proposed GaN AC/DC converter experimental prototype is shown in Fig. 10. Future work is being developed for verifying the feasibility of this GaN based converter for bi-directional power flow. Kelvin source connection is employed for the GaN and the gate drivers' chips, and minimizing the layout parasitics for the prototype was taken into account for the developed experimental prototype.

TABLE II. HF TRANSFORMER DESIGN.

Power	350 VA
Input – output voltage	130 V – 117 V
Frequency	100 KHz
Efficiency	98.2 %
Core	Nanocrystalline Vitroperm W376-04
Wire	16/30 Served Litz wire
Number of turns	25 primary/ 22 secondary
Optimum flux density	0.16T
Volume	31.51 cm^3
Leakage inductance	11.5 µH
Magnetizing inductance	18.7 mH

Fig. 10. The fabricated GaN AC/DC Converter.

V. CONCLUSION

Highly efficient power electronics converters with high gravimetric- and volumetric-power densities are desired for future power supplies. The proposed power converter yields a close-to-unity power factor, low harmonic content (<5%), and high efficiency power supply for 120Vac to 48Vdc/60Vdc conversion, operating at 100 KHz for a 1.4 kW load. The equivalent model for the proposed topology, state space equations, transfer function, and controllers design are developed in this paper. Analysis and simulation have demonstrated the feasibility of the proposed power supply topology for battery charging application. Experimental demonstration is presented and being under testing for further work to verify the operation of the proposed GaN AC/DC topology.

REFERENCES

[1] Z. Liu, F. C. Lee, Q. Li and Y. Yang, "Design of GaN-Based MHz Totem-Pole PFC Rectifier," in IEEE Journal of Emerging and Selected Topics in Power Electronics, vol. 4, no. 3, pp. 799-807, Sept. 2016.

[2] He Li, Chengcheng Yao, Lixing Fu, Xuan Zhang and Jin Wang, "Evaluations and applications of GaN HEMTs for power electronics," 2016 IEEE 8th International Power Electronics and Motion Control Conference (IPEMC-ECCE Asia), Hefei, 2016, pp. 563-569.

[3] P. Jang and B. H. Cho, "Zero-voltage switching analysis of active-clamped forward converter with current-doubler rectifier," 2015 9th International Conference on Power Electronics and ECCE Asia (ICPE-ECCE Asia), Seoul, 2015, pp. 253-258.

[4] H. I. Hsieh, K. P. Huang and G. C. Hsieh, "Analysis and realization study of a 1-kW phase-shift full-bridge converter with current-doubler rectifier for battery charging," 2016 IEEE 8th International Power Electronics and Motion Control Conference (IPEMC-ECCE Asia), Hefei, 2016, pp. 439-444.

[5] V. Beldjajev, I. Roasto and D. Vinnikov, "Analysis of current doubler rectifier based high frequency isolation stage for intelligent transformer," 2011 7th International Conference-Workshop Compatibility and Power Electronics (CPE), Tallinn, 2011, pp. 336-341.

[6] U. Badstuebner, J. Biela, D. Christen and J. W. Kolar, "Optimization of a 5-kW Telecom Phase-Shift DC–DC Converter With Magnetically Integrated Current Doubler," in IEEE Transactions on Industrial Electronics, vol. 58, no. 10, pp. 4736-4745, Oct. 2011.

[7] L. Zhou, Y. Wu, "99% Efficiency True-Bridgeless Totem-Pol PFC Based on GaN HEMTs," Transphorm, Inc. EDN, June, 14th, 2017

[8] B. R. Lin, K. Huang and D. Wang, "Analysis and implementation of full-bridge converter with current doubler rectifier," in IEE Proceedings - Electric Power Applications, vol. 152, no. 5, pp. 1193-1202, 9 Sept. 2005.

[9] Erickson and Maksimovic, Fundamentals of Power Electronics, Kluwer, 2nd edition, 2000.

[10] S. Nigsch, M. Schlenk and K. Schenk, "Detailed analysis of a current-doubler rectifier for an LLC resonant converter with high output current," 2017 IEEE Applied Power Electronics Conference and Exposition (APEC), Tampa, FL, 2017, pp. 1748-1754.